Influence of pretreatment on Surface Interaction Between Cu and Anatase-TiO_2 in the simultaneous photoremediation of nitrate and oxalic acid

Haruna Adamu[a,b*], Alan J. McCue[a], Rebecca S. F. Taylor[c], Haresh G. Manyar[d] and James A. Anderson[a]

[a]Surface Chemistry and Catalysis Group, Materials and Chemical Engineering, School of Engineering, University of Aberdeen, AB24 3UE, UK.

*Tel: +2348065309319, Email: hadamu2@atbu.edu.ng

[b]Department of Environmental Management Technology, Abubakar Tafawa Balewa University, Bauchi, Nigeria

[c]School of Chemical Engineering and Analytical Science, The University of Manchester, The Mill, Sackville Street, Manchester, M13 9PL, UK.

[d]CenTACat, School of Chemistry and Chemical Engineering, Queen's University, Belfast, David Keir Building, Stranmillis Road, Belfast, BT9 5AG, UK.

Abstract

Copper-promoted anatase-type TiO_2 photocatalysts (2.5 wt% Cu) were prepared by wet impregnation onto TiO_2 which was pre-calcined at 600°C and the other not subjected to any thermal pre-treatment. In the latter case, the material was inactive for the photo-reduction of nitrate whereas 600°C pre-calcined TiO_2 yielded a material which was active for the same reaction. The surface properties of the materials were determined by BET Surface area, SEM TEM, XRD, XPS, TPR, UV-Visible diffuse reflectance, DTA, N_2O pulsed chemisorption and FTIR studies. The BET and XRD and DTA showed that pre-calcination of TiO_2 stabilised the support, but coalescence of particles was observed in TiO_2 that was not subjected to any thermal pre-treatment as evidenced by crystallite growth. Similarly, XPS, FTIR and TPR proved the formation of Cu_2O particles on the surface of pre-calcined TiO_2. On the other hand, the absence of pre-calcination step resulted in interring of Cu species within the grown anatase crystallites that hindered their proper distribution over TiO_2, helped in its inactiveness in the photoreduction of nitrate. However, the prepared material using pre-calcined TiO_2 showed the overall nitrate and oxalic acid removal efficiency of 31 and 70% with N_2 and $NH4^+$ selectivity of 44.9 and 55.1 %, respectively. The results provide insight into the significance of activity-structure relation, inferring that the two surfaces were chemically not similar. Thus, as even supported by adsorption experiment, difference in photocatalytic behaviour amongst the prepared materials was a function of crystallinity, particle size, absence of surface defect and high energy sites.

Keywords: Nitrate, oxalic acid, photoremediation, metal oxide-support interaction, photocatalyst.

1 Introduction

The interaction between metal oxides and metal oxide semiconductors has been a subject of interest in heterogeneous photocatalysis for many years. This is not necessarily because the metal promoted metal oxide semiconductors have shown wide applications as photocatalysts for environmental clean-up, but also because there are still a variety of diverse explanations on the nature and activity-structure relationship between dispersed metal oxides on various metal oxide semiconductors.[1] Among the various metal oxide semiconductors, TiO_2 has appeared to be the most promising, environmentally compatible and widely used semiconductor in heterogeneous photocatalysis. Consequently, TiO_2 and its impregnated metal oxide-based have found different applications in environmental pollution remediation such as photocatalysts used for water denitrification in the presence of an organic hole scavenger.[2]

The photocatalytic process for environmental pollution abatement is based on the reactive properties of electron-hole pairs that are generated by UV-Vis illumination with energy greater than the semiconductor band gap.[3] These photogenerated electrons and holes have redox potential and can reach the semiconductor surface and react with adsorbed species rendering them benign.[4] However, photogenerated electrons/holes are also prone to recombination and it has been reported that TiO_2 suffers from rapid recombination which limits optimal photocatalytic potential.[5,6] In order to overcome such a challenge, one common approach that has received much attention is doping of crystalline TiO_2 with metal ion oxides, which suppress the rate of recombination and extends their lifetime of electron-hole pairs.[7,8]

The manifestation of the adverse detrimental effect of excessive amount of nitrate and its metabolites in surface and ground water bodies has coerced the international environmental protection agencies and health organisations to set tolerable limits for these pollutants. In recognition of the toxicity of nitrate and its metabolites, the World Health Organisation (WHO) and the U.S. Environmental Protection Agency (USEPA) have set the maximum tolerable contamination level of 10 mg L^{-1} of NO_3^- in drinking water source.[9,10] In the same vein, the European Union (EU) has recommended levels of 50, 0.1 and 0.5 mg L^{-1} to be the maximum permissible concentrations of NO_3^-, NO_2^- and NH_4^+ in water bodies against pollution, respectively.[11] In addition to the legislative control of nitrate pollution in surface and ground water sources, a large number of treatment techniques have been developed and tested amongst which the heterogeneous photocatalytic reduction of nitrate in the presence of an organic hole

scavenger has appeared to be promising and viable, as it can be operated at low cost and possibly installed in remote locations.[12,13] Despite the potential treatment ability of TiO_2 in the abatement of air and water pollution, TiO_2-P25 alone has been reported to show either no activity for this reaction[14,15] or relatively low activity but high selectivity for N_2 [16] or mainly produce NH_4^+ as an undesired product.[17] This has provoked attempts to modify TiO_2 with metals, which include Pt,[14,18,19] Pd,[14,19,20] Rh,[19] Au,[12,13] Ag,[16,21-23] Cu,[20,21,24,25] Cr and Zn.[25] Unlike TiO_2-P25, modification of the anatase-type TiO_2 (Hombikat UV 100) with Cu metal has been reported to be detrimental to the activity of the photocatalyst and selectivity to N_2 was reduced and in some cases was zero after addition of Cu[21,25]. This variation in terms of the impact of Cu was attributed to Cu particle size effects in addition to blockage of reactive sites on the surface of TiO_2.[21] These observations could be related, at least in part with the crystallinity of both the supported-metal and the support. The difference in the photocatalytic behaviour between the two supports may be related with the fact that TiO_2-P25 is a fully crystalline material, whereas Hombikat may consist of only 66% crystalline TiO_2 with the remaining part amorphous.[26] The later may contain defects which could serve as electron-hole recombination sites. The presence of such amorphous materials may serve as an electron or/and electron-hole pair trap which prevents electrons from participating in the reduction of nitrate and/or at the same time deteriorates the degradation process of the organic hole scavenger. In this study, Cu was chosen as the metal oxide co-catalysts with TiO_2 due to its natural abundance and low cost compared to noble metals such as Au, Ag and Pt and to the diverse range of results obtained to date using coper in its multiple forms.[21,65] Oxalic acid was selected as organic hole scavenger, although other acids such as formic acid are also often generated, as one of the incomplete mineralisation products of advanced oxidation treatments (AOTs) characterised as recalcitrant to the treatment system.[2,27]

The aim of this work was to investigate the photocatalytic performance of TiO_2-Hombikat and its Cu impregnated forms in an effort to explore, in greater detail, the surface chemistry of the materials using different physicochemical characterisation techniques and their solid-state behaviour with respect to photocatalytic reduction of nitrate in the presence of oxalic acid as an organic hole scavenger.

2 Experimental

2.1 Preparation of photocatalysts

All photocatalysts were prepared by wet impregnation method. TiO_2-UV100 (Hombikat, Sachtleben Chemie) was dispersed in ultra-pure deionised water (MilliQ ≥ 18.2 MΩ-cm) and stirred for 1 h before slow addition of an appropriate amount of $Cu(NO_3)_2.3H_2O$ in aqueous solution. This was stirred vigorously for 2 h before water was removed by evaporation to produce a paste. This was then dried at 60°C for 24 h before being calcined at 400°C for 2 h. Another sample was prepared following the same procedure except that TiO_2 was firstly pre-calcined at 600°C for 4 h before Cu impregnation. All the materials contained the same nominal Cu loading (2.5 wt%) and were labelled as Cu/TiO_2 and $Cu/600TiO_2$, of which the latter supported on the pre-calcined TiO_2. In order to investigate the significance of the preparation stage involving the incorporation of copper, materials were also prepared following the facile ethanol reduction method[28] to synthesise Cu_2O supported on TiO_2. Briefly, TiO_2 was dispersed in anhydrous ethanol before $Cu(NO_3)_2.3H_2O$ (2.5 wt%) was slowly added. After vigorous stirring for 2 h, the solvent was evaporated by drying at 60°C for 6 h before calcination at 350°C for 2 h. As before, an equivalent material was prepared following the same procedure but using 600°C pre-calcined TiO_2. In this case, samples were labelled as Cu_2O/TiO_2 and $Cu_2O/600TiO_2$, of which the latter was prepared using the pre-calcined TiO_2.

2.2 Characterisation

The crystal structure of the prepared photocatalysts was examined using a X'Pert Pro Diffractometer (PANalytical) with a Cu Kα radiation source (λ = 0.15418 nm) in the range 5-80° 2θ. Textural properties (surface area, pore volume and pore size) were determined by collecting N_2 adsorption-desorption isotherms at -196°C on a Tristar-3000 instrument (Micromeritics). To understand the changes which arose from pre-calcination treatment at 600°C, copper containing samples supported on TiO_2 which was either uncalcined or pre-calcined at 600°C were compared by differential thermal analysis (DTA) under a flow of air on a thermal analyser (STA 780). Profiles were collected in the temperature range 25-400°C using a 5°C ramp rate, although data is presented in the range 100-400°C as the only process observed below 100°C was the endothermic removal of water. This was done to mimic calcination and post-calcination scenarios of uncalcined and pre-calcined Cu-containing amaterials. The surface texture of the photocatalysts was captured by field emission scanning electron microscopy (FESEM) using a SUPRA 40VP microscope (Carl Zeiss NTS GmbH, Oberkochem) and the morphology of the materials was observed by high resolution

transmission electron microscopy (HRTEM) using a JOEL JEM-2000 EX microscope. The optical properties of the photocatalysts were studied using a UV-Visible spectrometer (Cary 60, Varian) in diffuse reflectance mode using a 60 mm diameter integrated sphere and $BaSO_4$ as the internal reference standard. To establish whether Cu changed the band gap of TiO_2 in the photocatalysts, $(\alpha h\nu)^{1/2}$ *versus* E_{photon} was applied by fitting the absorption data to the equation.

Reducibility of the photocatalysts was investigated by temperature-programmed reduction (TPR) using a TPDRO 1100 instrument equipped with a TCD detector. Samples were heated from 40 to 600°C at 5°C/min in 5% H_2/N_2. The amount of hydrogen consumed was quantified based on a response factor determined from a CuO reference standard. The dispersion of Cu on the supports was estimated by N_2O pulsing conducted using the same instrument.[29] Samples were firstly reduced at 300°C for 30 min before allowed to cool to 110°C. N_2O pulses (0.285 ml loop size, NTP) were subsequently exposed to the reduced sample. Unreacted N_2O was condensed in a liquid nitrogen trap and N_2 produced *via* decomposition/surface oxidation ($N_2O + 2\ Cu \rightarrow Cu_2O + N_2$) was measured using a TCD. The amount of N_2 produced was quantified based on a response factor determined from pulses of pure N_2. The dispersion (%) was calculated as the ratio of surface Cu atoms and total Cu measured by atomic absorption spectroscopy after sample digestion.[30,31]

The nature of the Cu species on the surface of the supports was probed by adsorption of CO using FTIR (1750 series spectrometer, Perkin-Elmer). Sample as self-supporting discs were suspended in a quartz holder in a vacuum line which permitted heating, out-gassing and gas manipulation. Sample was first evacuated and then heated to 120°C to remove surface water. The sample was cooled to room temperature and the cell evacuated to a residual pressure of *ca*. $4x10^{-5}$ Torr before an initial spectrum (25 scans, 4 cm^{-1} resolution) was collected prior to introduction of increasing CO pressures (0.2-50 Torr). Results are presented as difference spectra relative to the initial scan collected prior to exposure of CO. Additionally, a separate experiment was conducted to determine whether the presence of CO transformed Cu^{2+} to Cu^{+} at room temperature. In this case, a sample was evacuated at room temperature for 1 h, followed by exposure to CO (50 Torr). Spectra were collected after 5, 20, 40 and 60 min exposure to follow evolution of absorption bands indicative of both adsorbed CO and gaseous CO_2.

XPS measurements were carried out using a Kratos AXIS Ultra DLD XPS spectrometer with monochromated AlKα X-rays and hemispherical analyser with a pass energy of 160 eV. The powdered samples were mounted on copper tape and binding energies were normalised to

the C 1s signal from adventitious carbon at 284.6 eV. Background subtraction was performed using a Shirley background and Casa XPS.[32]

2.3 Adsorption of reagents tests

The adsorption of oxalic acid and nitrate were determined individually at constant temperature (25 ± 0.1°C) and without pH adjustment using different initial concentrations. 0.25 g of Cu/TiO_2 or $Cu/600TiO_2$ photcatalysts was added to 100 ml Pyrex bottles containing 25 ml of nitrate (10-100 mg/L) or oxalic acid (0.001-0.010 mol/L) solution and shaken in a thermostat water bath for 24 h. The suspensions were centrifuged, filtered using a syringe filter (0.45 μm, Millipore) and then the equilibrium concentrations of nitrate using a spectroquant nitrate kit and oxalate were determined using a UV-visible spectrometer (Lambda 25, Perkin-Elmer) at 340 and 262 nm wavelengths, respectively. To determine the uptake of nitrate and oxalic acid, the amount of nitrate and oxalic acid adsorbed per unit mass of sample (mol/g) was calculated using mathematical expression (1):

$$q_e = \frac{(C_i - C_e)}{m} V \qquad \textbf{(1)}$$

where q_e is the amount adsorbed at equilibrium (mol/g), C_i is the initial concentration (mol/L)**,** C_e is the solution equilibrium concentration (mol/L), V is the volume of the aqueous phase (L), and m is the mass of the sample used. Regression Chi-square (χ^2) test was employed as a criterion for fitting quality of an adsorption isotherm model.[33] The chi-square can be represented by the following equation:

$$\chi^2 = \sum \left[\frac{(qee - qec)2}{qec} \right] \qquad \textbf{(2)}$$

where q_{ee} is the equilibrium capacity of the adsorbent obtained from experiment (mol/g), and q_{ec} is the calculated equilibrium uptake according to the model (mol/g). A low value of χ^2 indicates that experimental data provides a good quality fit to the value from the model.

2.4 Photocatalytic tests

Photocatalytic reactions were carried out in a stirred, batch reactor fitted with a primary cooler (Fischer Scientific 3016S) to maintain the reaction temperature around 25°C. A secondary cooling system was also incorporated to control heat given out by the UV lamp

(Hereaus BQ 512 E, 400 W, 230 V and maximum wavelength of 365 nm). Water was used as the coolant in this secondary cooling system by providing a constant flow through a Pyrex cooler which encased the UV lamp. The Pyrex glass sleeve also functioned to filter out light of wavelengths below 290 nm which might otherwise lead to direct photolysis of nitrate and oxalic acid (Fig. 1). Therefore, only light in the range between 290 and 365 nm were available for the experiments conducted (Fig. SI-1). The temperature of the reaction was monitored by thermometer inserted in the reactor. Initially, 0.5 g/L photocatalyst was stirred in 1.5 L of ultra-pure water and N_2 bubbled for 30 min to displace any dissolved oxygen. Thereafter, 100 ml stock solutions of nitrate and oxalic acid were added to the suspension to give initial concentrations of 100 ppm nitrate and 0.005 M oxalic acid. The reactor was stirred for another 1 h in the dark, to attain adsorption-desorption equilibrium. A sample was then taken to determine the equilibrium concentrations of the model pollutants in solution before the light was turned on. During the photocatalytic reaction test, samples were withdrawn at fixed time intervals over a 3 h reaction period and filtered with a 0.45 µm syringe filter. The concentrations of nitrate, nitrite and oxalate were measured using ion chromatography (Dionex DX-120), while ammonium concentration was measured using a Merck Spectroquant test kit which follows the indophenol test for ammonium.[34] Thereafter, the degradation (%) of both model pollutants was calculated using equation 3.

$$\text{Degradation (\%)} = \frac{C0 - C_t}{C_0} \text{ x } 100 \quad \textbf{(3)}$$

where C_0 stands for the initial concentration at zero time of illumination, C_t is the concentration at a particular time of illumination. The selectivity toward N_2 (S_{N2}) was determined based on a nitrogen balance, evaluated from the balance of nitrogen by-product (NH_4^+) analysed in the reaction solution, according to equation (4 and 5).[22]

$$S(_{NH4}^{+}) = [NH_4^+]_t \,/\, ([NO_3^-]_0 - [NO_3^-]_t) \quad \textbf{(4)}$$

$$S(_{N2}) = ([NO_3^-]_0 - [NO_3^-]_t - [NH_4^+]_t) \,/\, ([NO_3^-]_0 - [NO_3^-]_t) \quad \textbf{(5)}$$

where $[X]_0$ is the concentration at time = 0 and $[x]_t$ is the concentration at time = t.

3 Results and discussion

3.1 Characterisation of photocatalysts

The XRD patterns of all the materials are shown in Fig. 2 with intense peaks apparent at 25.3, 37.9, 48.1, 54.0, 55.1, 62.8, 70.3 and 75.1° 2θ. These peaks correspond to the (101),

(004), (200), (105), (211), (213), (202) and (215) crystal planes of the anatase phase of TiO_2 (ICDD-01-075-2550). Although all the materials consisted of typical anatase phase, but sharp peak intensity and thin diffraction peaks in $600TiO_2$ and $Cu/600TiO_2$ were observed, suggesting a richer content of anatase phases and larger particle sizes compared to TiO_2, Cu/TiO_2. No diffraction peaks associated with rutile were observed even after pre-calcination at 600°C. No Cu species were detected, probably due to the low Cu loading. The crystallite sizes of all the materials were calculated by the application of the Scherrer equation and are displayed in Table 1. Pure TiO_2 has a relatively small crystallite size of 9.4 nm. A large increase in crystallite size (*ca*. 26 nm) was apparent following impregnation of Cu and subsequent calcination at 400°C for 2 h. Similarly, an increase in crystallite growth was observed following pre-calcination of TiO_2 at 600°C for 4 h, but no significant change in crystallite size was noted following subsequent loading of Cu over the support (Table 1), reflecting that the pre-calcined TiO_2 support was virtually stable during impregnation and post-calcination processes.

Nitrogen adsorption-desorption isotherms for all materials were collected to understand the impact of pre-calcination, calcination and post-calcination on the surface area and textural properties of the prepared materials. All samples display type IV isotherms according to IUPAC classification[35] (Fig. 2) with relatively faint hysteresis loops associated with capillary condensation in relatively small mesopores.[36] The BET surface area (S_{BET}), pore volume and pore size distributions of the materials are tabulated in Table 1. The surface area of pure TiO_2 was initially high (290 m^2/g) with a decrease to119 m^2/g after the addition of Cu and subsequent calcination. This could be attributed to poor thermal stability of the anatase-type TiO_2[37] and was responsible for the coalescence of particles that led to the decrease of surface area.[38] In addition, the loss of active surface area by the agglomeration of small crystallites into larger ones was also notably accompanied by loss of pore volume (Table 1). This decrease is consistent with crystallite growth observed from XRD. Pre-calcination of TiO_2 at 600°C led to a reduction in surface area from 290 to 99 m^2/g, however, this essentially remained constant even after the formation of $Cu/600TiO_2$, which implies that the pre-calcined TiO_2 phase was relatively stable even before the impregnation of Cu and after post-calcination treatment. So, the difference between the two materials was that significant structural changes were observed in the material where Cu was anchored on TiO_2 for the formation of Cu/TiO_2 without pre-calcination treatment. On the pore size distribution, the distributions lie within the range of 2-20 nm (Fig. 3a and b inserts) reflecting the mesoporous nature of all materials. The average pore sizes of the prepared Cu/TiO_2, $600TiO_2$ and $Cu/600TiO_2$ were found to be greater than

that of pure TiO_2, which could be an advantage to the adsorption-desorption processes on the surface of the materials. After the pre-calcination treatment and combination of TiO_2 with Cu, the pore size distribution broadened significantly, even though TiO_2 show a very narrow range of pore size distribution (Fig. 3 inserts) and thus, confirm the hybrid surface structure of the Cu/TiO_2, $600TiO_2$ and $Cu/600TiO_2$. Consequently, the pore size distribution of these materials comprised a small amount of micropores and the majority as mesopores. Interestingly, for comparison, the pore size distributions of $600TiO_2$ and $Cu/600TiO_2$ remained unchanged (Fig. 3b insert), which is in contrast with TiO_2 and Cu/TiO_2 (Fig. 3a insert) with no pre-calcination treatment. This indicates the relative stability of the Cu-containing material formed with pre-calcined TiO_2.

Figure 4 shows the exothermic DTA features observed during heating under air for Cu/TiO_2 and $Cu/600TiO_2$ samples, which are materials containing Cu supported on uncalcined and pre-calcined TiO_2, respectively. The Cu/TiO_2 profile shows an exothermic process occurring at *ca.* 320°C. The exothermic process observed is attributed to crystal growth of anatase that resulted in the sharpening of diffraction lines (Fig. 1 and Table 1) and reduction in BET area (Table 1). This similar observation has also been reported in the literature.[38] The equivalent transition was not apparent for the sample prepared with pre-calcined TiO_2, suggesting that the as-prepared $Cu/600TiO_2$ was relatively stable.

The surface texture and morphologies of Cu/TiO_2 and $Cu/600TiO_2$ captured by SEM and TEM are displayed in Fig. 5. The SEM micrographs show that Cu/TiO_2 (Fig. 5a) and $Cu/600TiO_2$ (Fig. 5b) exhibited subtle differences, of which $Cu/600TiO_2$ appeared to be more dispersed and homogeneous in terms of size and shape than Cu/TiO_2 which was more agglomerated. However, the TEM images for Cu/TiO_2 (Fig. 5c) and $Cu/600TiO_2$ (Fig. 5d), show no obvious differences between the two materials. The images extracted only prove the manifestation of TiO_2 crystallites, as there are no obvious signs of other crystalline phases, such as e.g. Cu. The inability of TEM technique to demarcate or detect the copper-containing phases may be related to the low Cu content in the two materials or due to the lack of contrast between Cu and TiO_2.

The optical absorption as a function of photon energy are shown in Fig. 6 for Cu/TiO_2 and $Cu/600TiO_2$. The material which was calcined at 400ºC after addition of Cu showed the same band gap of3.20 eV as the pure TiO_2 and consistent with the expectation for the anatase phase of TiO_2.[39-41] This suggests that impregnation of Cu on TiO_2 resulted in no effect on the electronic properties of the Cu-containing material formed. In contrast, the band gap of Cu-containing material which its support was pre-calcined at 600ºC prior to Cu impregnation, i.e.

$Cu/600TiO_2$ showed some deviation from that of pure TiO_2. The band gap of such material ($Cu/600TiO_2$) was significantly narrowed to3.12 eV, which implies electronic interactions between Cu and the solid support that led to charge transfer transitions between the d-electrons of Cu and valence and/or conduction bands of TiO_2.

In situ FTIR spectroscopy of adsorbed CO was employed to determine the nature of the surface of the exposed Cu species. It has been well established that CO adsorbed onto Cu^{2+} sites shows a band at 2200 cm^{-1},[42] whereas peaks due to CO on Cu^+ species and Cu^0 appear at 2102-2133 and 2060-2080 cm^{-1}, respectively.[42-47] Fig. 7a shows the spectra of adsorbed CO on the $Cu/600TiO_2$ sample. The main absorption band occurred at 2110 cm^{-1} and thus is attributed to adsorption on Cu^+ which is thought to be the predominant oxidation state. A small band was observed at *ca* 2060 cm^{-1} and suggests the presence of a small population of Cu^0 sites. Note, however, that band area due to CO on these sites is not a reflection on relative amounts due to the differences in relative molar absorption coefficients,[43] meaning that the Cu^0Cu^+ population is likely to be underestimated by relative band areas. In addition, the differences for the molar absorption coefficients of CO on Cu^+ and Cu^0 overemphasise the relative abundance of Cu^+ sites.[43] In contrast, the Cu/TiO_2 photocatalyst was not adsorbed CO to the same extent as the former (Fig. 7b), of which only a weak band observed at *ca*. 2115 cm^{-1} (*ca*. 40-fold less intense than observed for $Cu/600TiO_2$). In the same vein, Cu_2O/TiO_2 exhibited very similar behaviour as Cu/TiO_2 where CO was too faintly adsorbed over it (Fig.7d), which was signified with a weak band observed at *ca* 2120 cm^{-1} (*ca*. 60-fold less intense than observed for $Cu_2O/600TiO_2$ of Fig. 7c). From this, it is inferred that the availability of surface Cu sites must be different from materials which were formed with pre-calcined TiO_2. Also, no evidence of Cu^0 was observed in the sample of Cu/TiO_2. The acquired FTIR spectra of $Cu_2O/600TiO_2$ and Cu_2O/TiO_2 shown similarities to spectra of $Cu/600TiO_2$ and Cu/TiO_2, respectively (Fig. 7c and d). None of these samples exhibited a peak that could be assigned to CO adsorbed on Cu^{2+}. This may be because that copper in this oxidation state was not present, or was readily reduced either under vacuum, or in the presence on CO. To distinguish between the two likely situations, a sample of $Cu/600TiO_2$ was outgassed at beam temperature and exposed to CO. Spectra were collected over 1 h period but no change to the CO absorption bands or evidence of CO_2 formation (i.e., $2CuO + CO \rightarrow Cu_2O + CO_2$) was observed (Fig. 7e). This suggests that CO was not responsible for reducing Cu^{2+} at beam temperature, contrary to earlier reports.[45,47]

In order to understand the reducibility of Cu in the different samples, TPR profiles were collected (Fig. 8). The materials prepared after the pre-calcination treatment of the TiO_2 powder namely $Cu/600TiO_2$ and $Cu_2O/600TiO_2$ show TPR patterns characterised by the onset of

reduction at temperatures below 200°C. In contrast, the materials of Cu/TiO_2 and Cu_2O/TiO_2 show an onset of reduction above 200°C and full reduction of the latter was not completed until *ca.* 300ºC. The reduction peaks of $Cu/600TiO_2$ and $Cu_2O/600TiO_2$ that appeared below 200 °C can be assigned to Cu species that are readily reduced due to its high dispersion on the support. On the contrary, the reduction peak of Cu/TiO_2 above 200°C and full reduction of Cu_2O/TiO_2 that was not completed until ca 300ºC could be related to reduction of Cu species that were weakly interacted with the TiO_2 support. In addition, the broadness of their peaks perhaps resulted from the nature of the interaction of Cu species with the supports, i.e. TiO_2 with no pre-calcination treatment, upon which Cu species were either loosely held or no interaction with the support. It is also interesting to note that materials which displayed features due to adsorbed CO in the FTIR (Fig. 7a and c) are those which were reduced at lower temperatures (i.e. those materials prepared with pre-calcined TiO_2). In contrast, materials that gave rise to very low intense FTIR features due to adsorbed CO (Fig. 7b and d) required higher temperatures for the onset of reduction. These differences in behaviour amongst the materials may be associated with Cu accessibility, which conspicuously reflect the fact that the as-prepared materials derived from TiO_2 pre-calcined at 600ºC perhaps contained copper in a lower oxidation state and/or contained surface with no defects that reduced the probability of creating more difficult to reduce Cu species supported on pre-calcined TiO_2. The amount of hydrogen consumed was quantified and used to calculate percentage reduction assuming Cu was initially present as CuO (Table 2). On this basis, all materials exhibited degrees of reduction below 50% suggesting that copper was initially more likely present as Cu_2O. The presence of Cu^+ in the as-prepared materials is consistent with FTIR of adsorbed CO (Fig. 7), more especially in the case of the materials involving pre-calcined TiO_2. Note that although the onset temperature of reduction for materials based on $600TiO_2$ were lower, these materials also exhibited the lowest overall degrees of reduction (Table 2) at *ca.* 32% compared with *ca.* 48%, suggesting potentially a lower initial average oxidation state, as proposed above.

It is reasonable to conclude that Cu^{2+} was absent in all the as-prepared photocatalysts. The reduction of CuO during the preparation stages conceivably originate from the redox reaction of $CuO + Cu \rightarrow Cu_2O$, as Cu can act as a reducing agent at high temperature (above 300°C) in air.[48,49] This was strengthened by FTIR of adsorbed CO results that support the presence of Cu^0 in the samples. Based on the results here, the calcination treatment probably induced the creation of Cu^0 followed by strong interaction between Cu^{2+} and Cu^0 ions, leading to the charge transfer. In support of this statement, this process is thermodynamically feasible by nature of the electronic environment of the two species, i.e. CuO and Cu. The ionic nature

of Cu^{2+} with electronic configuration of $[Ar]3d^9$ is more electronegative than Cu and thus, is readily to be reduced to Cu^+ by Cu whose electronic environment ($[Ar]4s^23d^{10}$) remained intact. On the account for the existence of Cu_2O in the samples tested, the electronic arrangement of Cu_2O ($[Ar]\ 3d^{10}$) is more symmetrical and stable than CuO and therefore, can coexist with TiO_2. Consequently, even though Cu particles on TiO_2 mostly exist in multiple oxidation states, it appeared in this study that Cu existed predominantly as Cu^+. Similar results have been reported where Cu loaded on TiO_2 was dominated by Cu^+ or in a mix with Cu^0 after calcination.[50,51] Comparable results have been reported regarding the presence of a lower oxidation state for Cu following high calcination temperatures, but no explanation for the formation of Cu_2O was made.[52]

One characteristic which was relatively similar for all materials was the Cu dispersion as accessed by N_2O decomposition. Although, FTIR of adsorbed CO indicated that Cu/TiO_2 and Cu_2O/TiO_2 samples were not readily adsorb CO, the N_2O decomposition tests for percentage dispersion of Cu in all the materials studied indicate no significant differences. This anomaly was a consequence of the fact that FTIR was performed on materials which were outgassed only whereas N_2O reaction was conducted on samples reduced at 300ºC, a treatment which led to a degree of uniformity that was introduced to the samples in terms of the nature of the Cu phase.

XPS analyses were conducted to gain insight into the nature of Cu ions in the two types of support. XP spectra of Cu 2p core level profiles of Cu/TiO_2, $Cu/600TiO_2$, Cu_2O/TiO_2 and $Cu_2O/600TiO_2$ are displayed in Fig. 9a-d, respectively. The Cu $2p_{3/2}$ characteristic peaks Cu^0, Cu_2O, and CuO are expected at 932, 932.7 and 933.6 eV [52], respectively. The Cu $2p_{3/2}$ and $2p_{1/2}$ binding energy values for $Cu/600TiO_2$, Cu_2O/TiO_2 and $Cu_2O/600TiO_2$ appeared at 930.2 and 951 eV, confirming the presence of Cu^+ in the materials (Fig. 9b-d). The species were present in the form of Cu_2O rather than Cu^0 or CuO, as Cu^+ (Cu_2O) does not exhibit Cu 2p satellite peaks since the 3d band of Cu_2O is filled ($3d^{10}$) and the 4s band is unoccupied.[53] However, in the case of the Cu/TiO_2, apart from the Cu $2p_{3/2}$ and $2p_{1/2}$ characteristic peaks of Cu^+, energy satellite structures are found between 936 and 942 eV (Fig. 8a), which are associated with Cu^{2+} species. This very weak satellite peak found in the sample of Cu/TiO_2 confirms that very small quantities of Cu^{2+} were present, and conceivably existed as residues of the Cu^{2+} present during Cu_2O nanoparticle formation on the surfaces of TiO_2 and $600TiO_2$ supports. Therefore, this material may be compared with data for the reduction of nitrate in the presence of oxalic acid using copper based photocatalysts where Cu existed predominantly in a zero or plus two oxidation state.[14,15,20,21,24]

3.2 Adsorption isotherms of nitrate and oxalic acid

Adsorption isotherms were measured to assess interactions of nitrate and oxalic acid with the surface of Cu/TiO_2 and $Cu/600TiO_2$ photocatalysts. Pre-adsorption of reactants on the photocatalyst surface is of importance, since it can result in rapid interfacial charge carrier trapping, thus avoiding recombination of electron-hole pairs and leading to effective photochemical conversion.[17] Experimental data was fitted to both Langmuir and Fruendlich models but a better fit was obtained using the former and as such, only data determined from that model is presented here.

Figure 10 displays the adsorption isotherms and corresponding Langmuir isotherm for Cu/TiO_2 and $Cu/600TiO_2$. The experimental adsorption capacity for each of the materials along with the Langmuir derived predicted maximum (q_{max}) and derived Langmuir constants are summarised in Table 3. Nitrate showed the higher Langmuir constant over both materials but the lower maximum uptake values (fewer but stronger sites). Both nitrate and oxalic acid uptake on Cu/TiO_2 was lower than for $Cu/600TiO_2$ despite the larger surface area of the former. The Langmuir constants for nitrate and oxalic acid adsorption on Cu/TiO_2 were higher, which implying stronger adsorption on this surface than for $Cu/600TiO_2$. Adsorption behaviour on metal oxide surfaces are influenced by multiple factors including crystallinity, particle size and oxygen deficiencies.[54] It is therefore inferred that pre-calcination of TiO_2 at 600°C led to the removal of defect and other high energy adsorption sites from the surface of the pre-calcined support and such might be responsible for its superior adsorption capacity.

3.3 Photocatalytic activity evaluation

Photocatalytic nitrate reduction tests using oxalic acid as a hole scavenger under UV light were measured and the results presented in Fig. 11a-b with derived parameters presented in Table 4. Under the conditions employed, TiO_2 alone both the pre-calcined and one with no thermal pre-treatment found to be inactive for nitrate reduction, but faintly active in the removal of oxalic acid with conversion *ca.* 20% in both cases (Table 4). The absence of nitrate conversion confirms that nitrate photolysis was not occurred under the employed experimental conditions, which Fig. SI-1 further supports such inference. Similar levels of oxalic acid removal but without nitrate reduction was also achieved using the Cu/TiO_2 sample, (Fig. 11a, Table 4). In contrast, $Cu/600TiO_2$ sample was able to remove significant amounts of both oxalic acid and nitrate with effective conversion of 70 and 31%, respectively. To determine whether the method of copper impregnation was significant, another material was prepared using a different route known to produce Cu(1) oxide.[28] Surprisingly, the formed Cu_2O/TiO_2

was tested on the same reaction and resulted in only 26% oxalic acid degradation still with no nitrate removal. On the other hand, reaction conducted with material where Cu_2O was formed on pre-calcined TiO_2 that produced $Cu_2O/600TiO_2$ resulted in 72 and 35% photoremediation of oxalic acid and nitrate, respectively (Fig. 11b). Relationships between all the materials tested (Fig. 11a and b) suggest that the method of Cu incorporation unto TiO_2 support played, at most, a minor role while the thermal pre-treatment of TiO_2 was crucial in creating active photocatalysts.

It is therefore believed that TiO_2 and $600TiO_2$ interacted in different extents with the Cu phases. Pre-calcination before impregnation of Cu produced a more crystalline TiO_2, which facilitated surface intimate contact between the two phases of the combined materials as adjudged by the reduced band gap in the presence of Cu. This arrangement provided effective materials for the simultaneous photoremediation of oxalate and nitrate. In contrast, without pre-calcination of TiO_2, significant aggregation of the TiO_2 particles occurred during the incorporation of the Cu phase and calcination resulted in a degree of phase mixing comprised of both amorphous and crystalline phases (scheme 1). The lack of activity of the photocatalysts prepared on TiO_2 without pre-calcination could be attributed to such mixed configuration of phases (scheme 1), where a high concentration of amorphous defects served as traps for photogenerated electrons or electron-hole pairs and consequently lowered the photon yields of the photocatalysts. The low photocatalytic activity for TiO_2 comprised of an amorphous phase has also been reported elsewhere where the effect was attributed to the capturing of photo-excited electron and positive hole at the defects situated on the surface and in the bulk of photocatalyst.[55] In contrast, pre-calcination of TiO_2 stabilised the support from aggregation and led to the formation of phase capable of supporting Cu_2O particles on the surface and facilitated the photocatalytic reduction of nitrate over the material (Scheme 1). Although adsorption isotherms (Fig. 10) confirmed nitrate uptake on Cu/TiO_2, but photocatalytic nitrate reduction was not observed. Therefore, appropriate surface interaction between copper oxide phase with TiO_2 support was vital for significant photoremediation of nitrate and oxalic acid simultaneously. The (low) conversion of oxalic acid with absence of nitrate reduction over the supports alone and Cu_2O/TiO_2 suggest that protons in solution acted as conduction band electron scavengers for the one electron transfer process, and this buttressed with the similar levels of conversion in all cases signifying that the support alone was performing this function.

Nitrite formation was not detected throughout the reduction process (Fig. 12a) and ammonium was the only by-product observed (Table 4), potentially suggesting that nitrate could be converted directly to N_2 and NH_4^+. However, Ranjit et al.[56] reported increased

ammonium following addition of nitrite, suggesting that the latter was an intermediate in the photocatalytic reduction of nitrate. To verify whether N_2 or/and NH_4^+ was produced by the reaction between liberated NO_2^-, the photoreduction reaction of NO_2^- as a starting reagent in the presence of oxalic acid was studied under the same conditions as employed for NO_3^-. In comparison, the rate of NO_2^- removal over the Cu/600TiO_2 photocatalyst was greater than of NO_3^-(see Fig. 12a and b), confirming that NO_2^- is the more reactive reagent and consequently may not be observed in a 2-step reduction process. Additionally, under the acidic conditions employed, nitrite may be converted to HONO that may be degraded *via* photolysis under the broad band radiation employed here.[57] Selectivity to NH_4^+ was much decreased (Fig. 12b) compared with nitrate photoreduction (Fig. 12a). Therefore, failure to detect nitrite in the photoreduction of NO_3^- suggests that NO_2^-, if produced during nitrate reduction, either underwent rapid reduction or banished *via* photolysis and perhaps produced either N_2 or NH_4^+ formation. The former scenario may predominately infer as the formation of NH_4^+ was higher than the evolvement of N_2, which may be due the unavailability of electrons for nitrite reduction due to the excess consumption by H^+ ions contributed by oxalic acid and also due to the absence of sufficient $CO2^{\bullet-}$ radicals in the process. In comparison with other studies in the literature, Au/TiO_2-Hombikat photocatalyst yielded only 16% nitrate conversion after 180 min,[12,13] which is 2 times less than the yield of conversion of NO_3^- and selectivity of N_2 recorded in the present work. In a similar work, addition of Cu to TiO_2 (Hombikat UV100) was reported to be detrimental to its activity,[21] which was not the same effect with the present work. In summary, pre-calcination atmosphere has been found to have significant effects on the photocatalytic activity of Cu-promoted TiO_2 (Hombikat UV100) in nitrate photoreduction. The pre-calcination resulted in removal of defect and high energy surface-active sites, leading to photocatalytic activity. Thus, as even supported by adsorption results, differences in photocatalytic behaviour amongst the prepared materials was a function of crystallinity, particle size, absence of surface defect and high energy adsorption sites.

It is believed that in the case of metal-supported TiO_2 photo-assisted nitrate reduction involves metal acting as an electron sink.[2,13,20,28] However, a composite involving Cu_2O and TiO_2 are active metal oxide semiconductors pairing in the present study, consistent with recent studies which demonstrated that the combined photocatalytic properties of Cu_2O and TiO_2 are beneficial.[28] The combination of p-type semiconductor (Cu_2O) with n-type semiconductor (TiO_2) form a heterojunction with an intrinsic electric field that favours separation of photogenerated electrons and holes.[28,58] When a photocatalyst containing Cu_2O and TiO_2 is illuminated, photogenerated electrons can move from the conduction band of Cu_2O into the

conduction band of TiO_2 (-0.45 V)[59] which is more positive than Cu_2O (-1.64 V).[60,61] In the same vein, photogenerated holes migrate from the valence band of TiO_2 to the valence band of Cu_2O (scheme 2). As the charge separation route is different from a conventional system of metal deposited on TiO_2 such as Cu/TiO_2 photocatalyst, the following mechanism involved in the photocatalytic reduction of nitrate in the presence of oxalic acid is proposed. Both Cu_2O and TiO_2 can be simultaneously photo-activated and generate electron-hole pairs in accordance with Equations 6 and 7:

$$TiO_2 + h\nu \longrightarrow e^- + h^+ \quad \textbf{(6)}$$

$$Cu_2O + h\nu \longrightarrow e^- + h^+ \quad \textbf{(7)}$$

This followed by consumptions of photogenerated electrons and holes by surface adsorbed nitrate and oxalate ions, respectively (scheme 2). In earlier investigations[14,15,17], it was reported that nitrate reduction in the presence of oxalate anion could proceed indirectly through formation of oxalate radical that decomposed to produce $CO_2^{\bullet-}$[62] (Equation 8). On the other hand, the one electron reduction of nitrate is not thermodynamically possible over TiO_2[57]. It has been shown that $CO_2^{\bullet-}$ species are much active and have strong reductive ability (E° (CO_2/ $CO_2^{\bullet-}$) = -1.8 V)[17], capable of reducing nitrate to N_2 (E° (NO_3^-/N_2) = 1.25 V) (Equation 9) or to ammonium (E° (NO_3^-/NH_4^+) = 1.203 V) (Equation 10).[14-16] It was also shown that photogenerated electrons on TiO_2 can reduce nitrate to N_2 or NH_4^+ in a five and eight-electron reduction, respectively, (Equation 11and 12).[22,63] In addition, independent conversion of NO_2^- to N_2 *via* a 3-electron reduction (Equation 13) was confirmed (Fig. 12b). The NO_2^- to N_2 reduction is thermodynamically favoured because the electrochemical potential of nitrite to N_2 (E° (NO_2^-/N_2) = 1.45 V) is more positive than the reduction potential for NH_4^+ formation (E° (NO_2^-/NH_4^+) = 0.897 V). The photoreduction of NO_3^- to N_2 may also proceed by further reduction of NO_2^- to N_2 (Equation 13). In addition, even though the formation of NH_4^+ occurred to a limited extent during the photoreduction reaction of NO_2^- (Figure 12b), conversion of NO_2^- to NH_4^+ was feasible during the photoreduction of nitrate and thus considered as part of the overall reaction mechanism (Equation 14). Previous studies have shown that $CO_2^{\bullet-}$ species has a stronger reductive ability compared to (E° (NO_2^-/N_2) = 1.45 V) as well as (E° (NO_2^-/NH_4^+) = 0.897 V)[16,64], and therefore is able to reduce NO_2^- to N_2 and likewise to NH_4^+, respectively (Equations 15 and 16).

$$C_2O_4^-{}_{ads} + h^+ \longrightarrow C_2O_4^{\bullet-} \longrightarrow CO_2^{\bullet-} + CO_2 \quad \textbf{(8)}$$

$$NO_3^-{}_{ads} + 5CO_2^{\bullet-} + 6H^+ \longrightarrow 1/2\ N_2 + 3H_2O + 5CO_2 \quad \textbf{(9)}$$

$$NO_3^-{}_{ads} + 8CO_2^{\bullet-} + 10H^+ \longrightarrow NH_4^+ + 3H_2O + 8CO_2 \quad \textbf{(10)}$$

$$NO_3^-{}_{ads} + 6H^+ + 5e^- \longrightarrow 1/2N_2 + 3H_2O \quad \textbf{(11)}$$

$$NO_3^-{}_{ads} + 10H^+ + 8e^- \longrightarrow NH_4^+ + 3H_2O \quad \textbf{(12)}$$

$$NO_2^-{}_{ads} + 4H^+ + 3e^- \longrightarrow 1/2N_2 + 2H_2O \quad \textbf{(13)}$$

$$NO_2^-{}_{ads} + 8H^+ + 6e^- \longrightarrow NH_4^+ + 2H_2O \quad \textbf{(14)}$$

$$NO_2^-{}_{ads} + 3CO_2^{\bullet -} + 4H^+ \longrightarrow 1/2N_2 + 2H_2O + 3CO_2 \quad \textbf{(15)}$$

$$NO_2^-{}_{ads} + 6CO_2^{\bullet -} + 8H^+ \longrightarrow NH_4^+ + 2H_2O + 6CO_2 \quad \textbf{(16)}$$

4 Conclusions

Thermally untreated TiO_2 (anatase) was found to be ineffective for the simultaneous photocatalytic removal of nitrate and oxalic acid, although the latter was photodegraded to a limited extent, probably involving a one electron transfer reaction involving protons and the generation of hydrogen. In the same vein, Cu-impregnated anatase-TiO_2 failed to produce an active material. However, the loading of Cu onto pre-calcined anatase-TiO_2 produced material which was able to photoremediate both nitrate and oxalic acid simultaneously. Active photocatalysts were those which contained readily reducible Cu_2O as deduced by TPR, FTIR and XPS. These active materials exhibited more than 30 and $\geq$ 70% photoremediation of nitrate and oxalic acid that favoured 55.1 and 44.9% selectivity of NH_4^+ and N_2, respectively. Although the difference amongst the two materials largely relied on the key role of the surface interaction between Cu^+ species and solid supports, adsorption capacity and relative adsorption strength differences were also partly considered played a role in inducing improved performance in terms of simultaneous photoremediation of nitrate and oxalic acid. Thus, understanding of surface characteristics in terms of activity-structure relation of a material serves to be a key route in the development of an improved photocatalyst.

Acknowledgements

This research work was partly supported by the Petroleum Technology Development Fund (PTDF) of Nigeria. We are grateful to Abubakar Tafawa Balewa University, Bauchi-Nigeria for the award of fellowship to Haruna Adamu.

References

1. Kochuveedu, S. T.; Jang, Y. H.; Kim, D. H. A study on the mechanism for the interaction of light with noble metal-metal oxide semiconductor nanostructures for various photophysical applications. *Chem. Soc. Rev.* **2013**, *42*, 8467-8493.

2. Shand, M.; Anderson, J. A. Aqueous phase photocatalytic nitrate destruction using titania based materials: Routes to enhanced performance and prospects for visible light activation. *Catal. Sci. Technol.* **2013**, *3*, 879-899.

3. Hoffmann, M. R.; Martin, S. T.; Choi, W.; Bahnemann, D. W. Environmental applications of semiconductor photocatalysis. *Chem. Rev.* **1995**, *95*, 69-96.

4. Linsebigler, A. L.; Lu, G.; Yates Jr., J. T. Photocatalysis on TiO_2 surfaces: Principles, mechanisms, and selected results. *Chem. Rev.* **1995**, *95*, 735-758.

5. Nebel, C. E. Photocatalysis: A source of energetic electrons. *Nature Mater.* **2013**, *12*, 780-781.

6. Wang, Z.; Cai, W.; Hong, X.; Zhao, X.; Xu, F.; Cai, C. Photocatalytic degradation of phenol in aqueous nitrogen-doped TiO_2 suspensions with various light sources. *Appl. Catal. B: Environ.* **2005**, *57*, 223-231.

7. Di Valentin, C.; Finazzi, E.; Pacchioni, G.; Selloni, A.; Livraghi, S.; Paganini, M. C.; Giamello, E. N-doped TiO2: Theory and experiment. *Chem. Phys.* **2007**, *339*, 44-56.

8. Byrappa, K.; Dayananda, A. S.; Sajan, C. P.; Basavalingu, B.; Shayan, M. B.; Soga, K.; Yoshimura, M. Hydrothermal preparation of ZnO:CNT and TiO_2:CNT composites and their photocatalytic applications. *J. Mater. Sci.* **2008**, *43*, 2348-2355.

9. U.S. Environmental Protection Agency Drinking Water Standards and Health Adversories, U. S. Environmental Protection Agency, Office of Water. **2000**, *822-B-00-001*.

10. WHO Chemical Fact Sheets- Nitrate and nitrite. **2003**, *pp. 417-420.*

11. EU Report from the Commission to the Council and the European Parliament. On implementation of Council Directive 91/676/EEC concerning the protection of waters against pollution caused by nitrates from agricultural sources based on Member State Reports for period 2004-2007. **2011**.

12. Anderson, J. A. Photocatalytic nitrate reduction over Au/TiO_2. *Catal. Today* **2011**, *175*, 316-321.

13. Anderson, J. A. Simultaneous photocatalytic degradation of nitrate and oxalic acid over gold promoted titania. *Catal. Today* **2012**, *181*, 171-176.

14. Gao, W.; Jin, R.; Chen, J.; Guan, X.; Zeng, H.; Zhang, F.; Guan, N. Titania-supported bimetallic catalysts for photocatalytic reduction of nitrate. *Catal. Today* **2004**, *90*, 331-336.

15. Jin, R.; Gao, W.; Chen, J.; Zeng, H.; Zhang, F.; Liu, Z.; Guan, N. Photocatalytic reduction of nitrate ion in drinking water by using metal-loaded $MgTiO_3$-TiO_2 composite semiconductor catalyst. *J. Photochem. Photobiol. A.* **2004**, *162*, 585-590.

16. Zhang, F.; Jin, R.; Chen, J.; Shao, C.; Gao, W.; Li, L.; Guan, N. High photocatalytic activity and selectivity for nitrogen in nitrate reduction on Ag/TiO_2 catalyst with fine silver clusters. *J. Catal.* **2005**, *232*, 424-431.

17. Li, Y.; Wasgestian, F. Photocatalytic reduction of nitrate ions on TiO_2 by oxalic acid. *J. Photochem. Photobiol. A.* **1998**, *112*, 255-259.

18. Hirayama, J.; Kamiya, Y. Combining the Photocatalyst Pt/TiO_2 and the Nonphotocatalyst SnPd/Al_2O_3 for Effective Photocatalytic Purification of Groundwater Polluted with Nitrate. *ACS Catal.* **2014**, *4*, 2207-2215.

19. Ranjit, K. T.; Viswanathan, B. Photocatalytic reduction of nitrite and nitrate ions to ammonia on M/TiO_2 catalysts. *J. Photochem. Photobiol. A.* **1997**, *108*, 73-78.

20. Kominami, H.; Nakaseko, T.; Shimada, Y.; Furusho, A.; Inoue, H.; Murakami, S. -.; Kera, Y.; Ohtani, B. Selective photocatalytic reduction of nitrate to nitrogen molecules in an aqueous suspension of metal-loaded titanium(IV) oxide particles. *Chem. Commun.* **2005**, 2933-2935.

21. Sá, J.; Agüera, C. A.; Gross, S.; Anderson, J. A. Photocatalytic nitrate reduction over metal modified TiO_2. *Appl. Catal. B: Environ.* **2009**, *85*, 192-200.

22. Doudrick, K.; Yang, T.; Hristovski, K.; Westerhoff, P. Photocatalytic nitrate reduction in water: Managing the hole scavenger and reaction by-product selectivity. *Appl. Catal. B: Environ.* **2013**, *136–137*, 40-47.

23. Ren, H.; Jia, S.; Zou, J.; Wu, S.; Han, X. A facile preparation of Ag_2O/P25 photocatalyst for selective reduction of nitrate. *Appl. Catal. B: Environ.* **2015**, *176–177*, 53-61.

24. Kominami, H.; Furusho, A.; Murakami, S. -.; Inoue, H.; Kera, Y.; Ohtani, B. Effective photocatalytic reduction of nitrate to ammonia in an aqueous suspension of metal-loaded titanium(IV) oxide particles in the presence of oxalic acid. *Catal. Lett.* **2001**, *76*, 31-34.

25. Luiz, D. d. B.; Andersen, S. L. F.; Berger, C.; José, H. J.; Moreira, R. D. F. P. M. Photocatalytic reduction of nitrate ions in water over metal-modified TiO_2. *J. Photochem. Photobiol. A.* **2012**, *246*, 36-44.

26. Jensen, H.; Soloviev, A.; Li, Z.; Søgaard, E. G. XPS and FTIR investigation of the surface properties of different prepared titania nano-powders. *Appl. Surf. Sci.* **2005**, *246*, 239-249.

27. Beltrán, F. J.; Rivas, F. J.; Montero-de-Espinosa, R. Iron type catalysts for the ozonation of oxalic acid in water. *Water Res.* **2005**, *39*, 3553-3564.

28. Li, Y.; Wang, B.; Liu, S.; Duan, X.; Hu, Z. Synthesis and characterization of Cu_2O/TiO_2 photocatalysts for H_2 evolution from aqueous solution with different scavengers. *Appl. Surf. Sci.* **2015**, *324*, 736-744.

29. McCue, A. J.; Anderson, J. A. CO induced surface segregation as a means of improving surface composition and enhancing performance of CuPd bimetallic catalysts. *J. Catal.* **2015**, *329*, 538-546.

30. Weir, A.; Westerhoff, P.; Fabricius, L.; Hristovski, K.; Von Goetz, N. Titanium dioxide nanoparticles in food and personal care products. *Environ. Sci. Technol.* **2012**, *46*, 2242-2250.

31. Lomer, M. C. E.; Thompson, R. P. H.; Commisso, J.; Keen, C. L.; Powell, J. J. Determination of titanium dioxide in foods using inductively coupled plasma optical emission spectrometry. *Analyst* **2000**, *125*, 2339-2343.

32. Shirley, D. A. High-resolution X-ray photoemission spectrum of the valence bands of gold. *Phys. Rev. B* **1972**, *5*, 4709.

33. Ho, Y. Selection of optimum sorption isotherm. *Carbon* **2004**, *42*, 2115-2116.

34. Bolleter, W. T.; Bushman, C. J.; Tidwell, P. W. Spectrophotometric determination of ammonia as indophenol. *Anal. Chem.* **1961**, *33*, 592-594.

35. Sing, K. S. W. Reporting physisorption data for gas/solid systems with special reference to the determination of surface area and porosity. *Pure Appl. Chem.* **1982**, *54*, 2201-2218.

36. Barrett, E. P.; Joyner, L. G.; Halenda, P. P. The determination of pore volume and area distributions in porous substances. I. Computations from nitrogen isotherms. *J. Am. Chem. Soc.* **1951**, *73*, 373-380.

37. Sun, C.; Zhu, J.; Lv, Y.; Qi, L.; Liu, B.; Gao, F.; Sun, K.; Dong, L.; Chen, Y. Dispersion, reduction and catalytic performance of CuO supported on ZrO_2-doped TiO_2 for NO removal by CO. *Appl. Catal. B: Environ.* **2011**, *103*, 206-220.

38. Oliveri, G.; Ramis, G.; Busca, G.; Escribano, V. S. Thermal stability of vanadia-titania catalysts. *J. Mater. Chem.* **1993**, *3*, 1239-1249.

39. Ahmed, S.; Rasul, M. G.; Martens, W. N.; Brown, R.; Hashib, M. A. Heterogeneous photocatalytic degradation of phenols in wastewater: A review on current status and developments. *Desalination* **2010**, *261*, 3-18.

40. Malato, S.; Fernández-Ibáñez, P.; Maldonado, M. I.; Blanco, J.; Gernjak, W. Decontamination and disinfection of water by solar photocatalysis: Recent overview and trends. *Catal. Today* **2009**, *147*, 1-59.

41. Fujishima, A.; Zhang, X.; Tryk, D. A. TiO_2 photocatalysis and related surface phenomena. *Surf. Sci. Reports* **2008**, *63*, 515-582.

42. Zhu, S.; Liang, S.; Tong, Y.; An, X.; Long, J.; Fu, X.; Wang, X. Photocatalytic reduction of CO_2 with H_2O to CH_4 on Cu(i) supported TiO_2 nanosheets with defective {001} facets. *Phys. Chem. Chem. Phys.* **2015**, *17*, 9761-9770.

43. Coloma, F.; Bachiller-Baeza, B.; Rochester, C. H.; Anderson, J. A. Infrared study of competitive crotonaldehyde and CO adsorption on Cu/TiO_2. *Phys. Chem. Chem. Phys.* **2001**, *3*, 4817-4825.

44. Boccuzzi, F.; Chiorino, A.; Martra, G.; Gargano, M.; Ravasio, N.; Carrozzini, B. Preparation, characterisation, and activity of Cu/TiO_2 catalysts: I. Influence of the preparation method on the dispersion of copper in Cu/TiO_2. *J. Catal.* **1997**, *165*, 129-139.

45. Wu, G.; Guan, N.; Li, L. Low temperature CO oxidation on Cu-Cu_2O/TiO_2 catalyst prepared by photodeposition. *Catal. Sci. Technol.* **2011**, *1*, 601-608.

46. Liu, L.; Zhao, C.; Li, Y. Spontaneous dissociation of CO_2 to CO on defective surface of Cu(I)/TiO_2- x nanoparticles at room temperature. *J. Phys. Chem. C* **2012**, *116*, 7904-7912.

47. Prestipino, C.; Regli, L.; Vitillo, J. G.; Bonino, F.; Damin, A.; Lamberti, C.; Zecchina, A.; Solari, P. L.; Kongshaug, K. O.; Bordiga, S. Local structure of framework Cu(II) in HKUST-1 metallorganic framework: Spectroscopic characterization upon activation and interaction with adsorbates. *Chem. Mater.* **2006**, *18*, 1337-1346.

48. Han, S.; Chen, H. -.; Chu, Y. -.; Shih, H. C. Phase transformations in copper oxide nanowires. *J. Vac. Sci. Technol. B Microelectron. Nanometer. Struct.* **2005**, *23*, 2557-2560.

49. Wang, W.; Varghese, O. K.; Ruan, C.; Paulose, M.; Grimes, C. A. Synthesis of CuO and Cu_2O crystalline nanowires using Cu $(OH)_2$ nanowire templates. *J. Mater. Res.* **2003**, *18*, 2756-2759.

50. Tseng, I.; Wu, J. C. S.; Chou, H. Effects of sol–gel procedures on the photocatalysis of Cu/TiO_2 in CO_2 photoreduction. *J. Catal.* **2004**, *221*, 432-440.

51. Tseng, I.; Wu, J. C. Chemical states of metal-loaded titania in the photoreduction of CO_2. *Catal. Today* **2004**, *97*, 113-119.

52. Lalitha, K.; Sadanandam, G.; Kumari, V. D.; Subrahmanyam, M.; Sreedhar, B.; Hebalkar, N. Y. Highly stabilized and finely dispersed Cu_2O/TiO_2: A promising visible sensitive photocatalyst for continuous production of hydrogen from glycerol:water mixtures. *J. Phys. Chem. C* **2010**, *114*, 22181-22189.

53. Yılmaz, S.; McGlynn, E.; Bacaksız, E.; Özcan, Ş; Byrne, D.; Henry, M. O.; Chellappan, R. Effects of Cu diffusion-doping on structural, optical, and magnetic properties of ZnO nanorod arrays grown by vapor phase transport method. *J. Appl. Phys.* **2012**, *111*, 013903-7.

54. Jegadeesan, G.; Al-Abed, S. R.; Sundaram, V.; Choi, H.; Scheckel, K. G.; Dionysiou, D. D. Arsenic sorption on TiO_2 nanoparticles: Size and crystallinity effects. *Water Res.* **2010**, *44*, 965-973.

55. Ohtani, B.; Ogawa, Y.; Nishimoto, S. Photocatalytic activity of amorphous-anatase mixture of titanium(IV) oxide particles suspended in aqueous solutions. *J. Phys. Chem. B* **1997**, *101*, 3746-3752.

56. Ranjit, K. T.; Varadarajan, T. K.; Viswanathan, B. Photocatalytic reduction of nitrite and nitrate ions to ammonia on Ru/TiO_2 catalysts. *J. Photochem. Photobiol. A.* **1995**, *89*, 67-68.

57. Tugaoen, H. O.; Garcia-Segura, S.; Hristovski, K.; Westerhoff, P. Challenges in photocatalytic reduction of nitrate as a water treatment technology. *Sci. Total Environ.* **2017**, *599-600*, 1524-1551.

58. Jiang, G.; Wang, R.; Jin, H.; Wang, Y.; Sun, X.; Wang, S.; Wang, T. Preparation of Cu_2O/TiO_2 composite porous carbon microspheres as efficient visible light-responsive photocatalysts. *Powder Technol.* **2011**, *212*, 284-288.

59. Zaban, A.; Micic, O. I.; Gregg, B. A.; Nozik, A. J. Photosensitization of nanoporous TiO_2 electrodes with InP quantum dots. *Langmuir* **1998**, *14*, 3153-3156.

60. Lei, M.; Wang, N.; Zhu, L.; Zhou, Q.; Nie, G.; Tang, H. Photocatalytic reductive degradation of polybrominated diphenyl ethers on CuO/TiO_2 nanocomposites: A mechanism based on the switching of photocatalytic reduction potential being controlled by the valence state of copper. *Appl. Catal. B: Environ.* **2016**, *182*, 414-423.

61. Adamu, H.; McCue, A. J.; Taylor, R. S.; Manyar, H. G.; Anderson, J. A. Simultaneous Photocatalytic Removal of Nitrate and Oxalic acid over Cu_2O/TiO_2 and Cu_2O/TiO_2-AC Composites. *Appl. Catal. B: Environ.* **2017**, *217*, 181-191.

62. Stanbury, D. M. Reduction potentials involving inorganic free radicals in aqueous solution. *Adv. inorg. chem.* **1989**, *33*, 69-138.

63. Gekko, H.; Hashimoto, K.; Kominami, H. Photocatalytic reduction of nitrite to dinitrogen in aqueous suspensions of metal-loaded titanium(iv) oxide in the presence of a hole scavenger: An ensemble effect of silver and palladium co-catalysts. *Phys. Chem. Chem. Phys.* **2012**, *14*, 7965-7970.

64. Li-Fen, L.; Xiao-Yan, D.; Feng-Lin, Y.; Yu, J. C. Photocatalytic reduction of nitrate by Ag/TiO_2 catalyst. *Chin. J. Inorg. Chem.* **2008**, *24*, 211-217.

Table 1 - Physical properties of the materials

Materials	S_{BET} (m^2/g)	Pore volume (cm^3/g)	Average pore size (nm)	[a]Crystallite size (nm)
Pure TiO_2	290	0.43	4.4	9.4
Cu/TiO_2	119	0.26	9.8	26.4
$600TiO_2$	99	0.30	9.7	32.8
$Cu/600TiO_2$	97	0.31	10.1	32.2

[a]As determined using Sherrer equation applied to XRD pattern

Table 2 – Physiochemical characteristics of copper species.

Materials	Nominal Cu wt%	Actual Cu wt%[a]	Dispersion (%)[b]	Reducible Cu (%)[c]
Cu/TiO_2	2.5	2.38	5.3	47
$Cu/600TiO_2$	2.5	2.16	5.4	31
Cu_2O/TiO_2	2.5	2.27	3.5	48
$Cu_2O/600TiO_2$	2.5	2.32	5.0	33

[a]Determined by AAS. [b]Based on N_2O pulsed chemisorption [c]Assuming Cu initially present as CuO.

Table 3 - Adsorption parameters for nitrate and oxalic acid.

Material	Adsorbate	Experimental max. amount Adsorbed mol/g	K_L (M^{-1})	q_{max} (mol/g)	R^2	χ^2
Cu/TiO_2	nitrate	$8.02x10^{-5}$	5329	$8.69x10^{-5}$	0.991	$5.17x10^{-7}$
	oxalic acid	$1.09x10^{-4}$	4151	$1.27x10^{-4}$	0.990	$5.47x10^{-7}$
$Cu/600TiO_2$	nitrate	$6.10x10^{-4}$	3417	$6.37x10^{-4}$	0.990	$6.99x10^{-7}$
	oxalic acid	$8.17x10^{-4}$	2348	$8.65x10^{-4}$	0.992	$1.69x10^{-7}$

Table 4- Conversion, rate constants and selectivities for nitrate/oxalic acid photodegradation.

Materials	Nitrate conversion (%)	Oxalate conversion (%)	Rate constant (min^{-1})		Final Ammonia selectivity (%)	Final Nitrogen selectivity (%)
			Nitrate	Oxalate		
TiO_2	0	19	-	0.0018	–	–
$600TiO_2$	0	22	-	0.0021	–	–
Cu/TiO_2	0	20	-	0.0020	–	–
$Cu/600TiO_2$	31	70	0.0019	0.0056	55.1	44.9
Cu_2O/TiO_2	0	26	-	0.0023	–	–
$Cu_2O/600TiO_2$	35	72	0.0023	0.0061	57.4	42.6

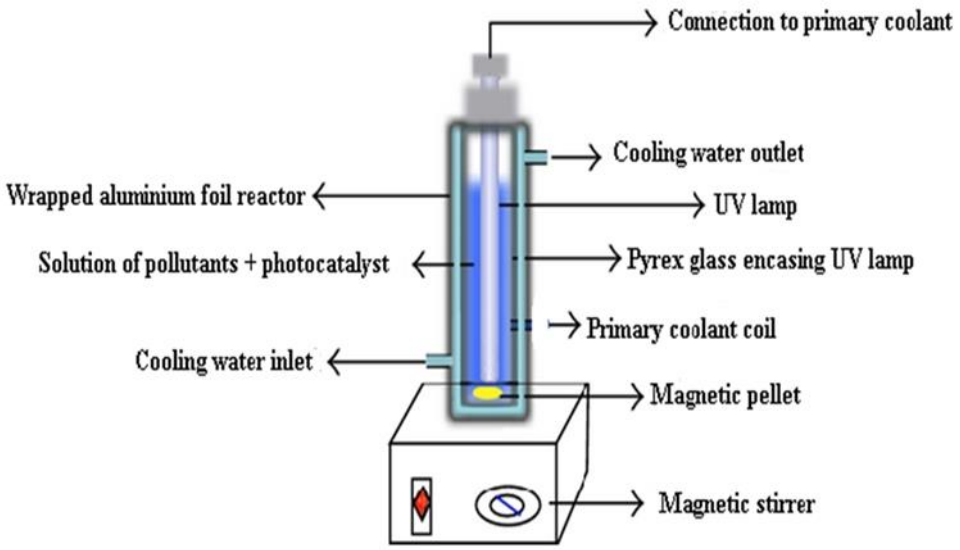

Figure 1- UV illumination experimental set-up for the photo-remediation of model pollutant(s) (nitrate and oxalic acid).

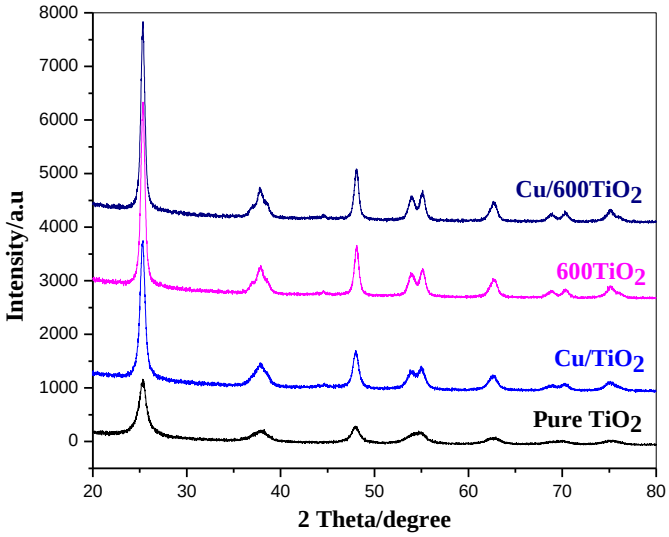

Figure 2 – powder XRD patterns of TiO_2, Cu/TiO_2, $600TiO_2$ and $Cu/600TiO_2$.

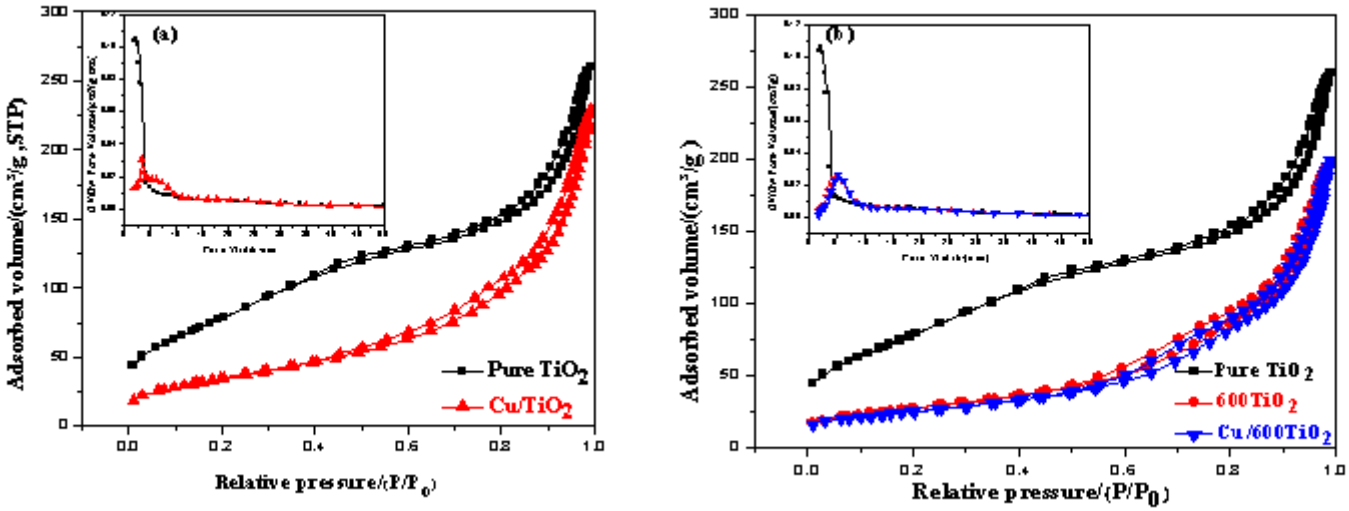

Figure 3 - Nitrogen adsorption-desorption isotherms of the materials with corresponding pore size distribution (insert). (a) Samples with no pre-calcination treatment and (b) samples with pre-calcination step at 600°C.

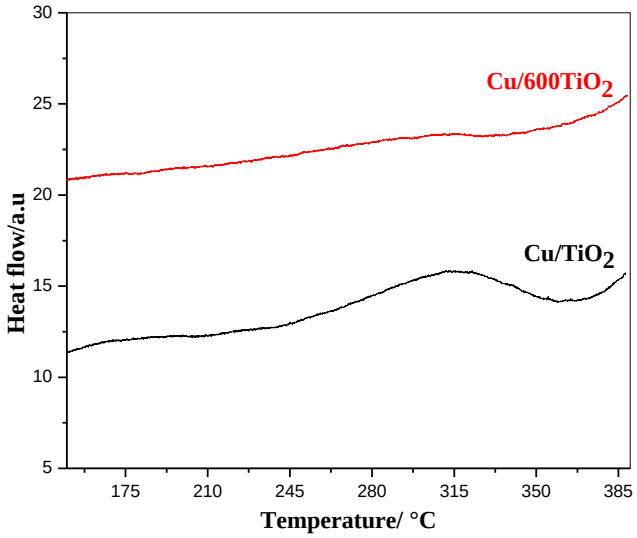

Figure 4 - DTA curves for uncalcined copper promoted titania (Cu/TiO_2) and precalcined copper promoted titania ($Cu/600TiO_2$) samples.

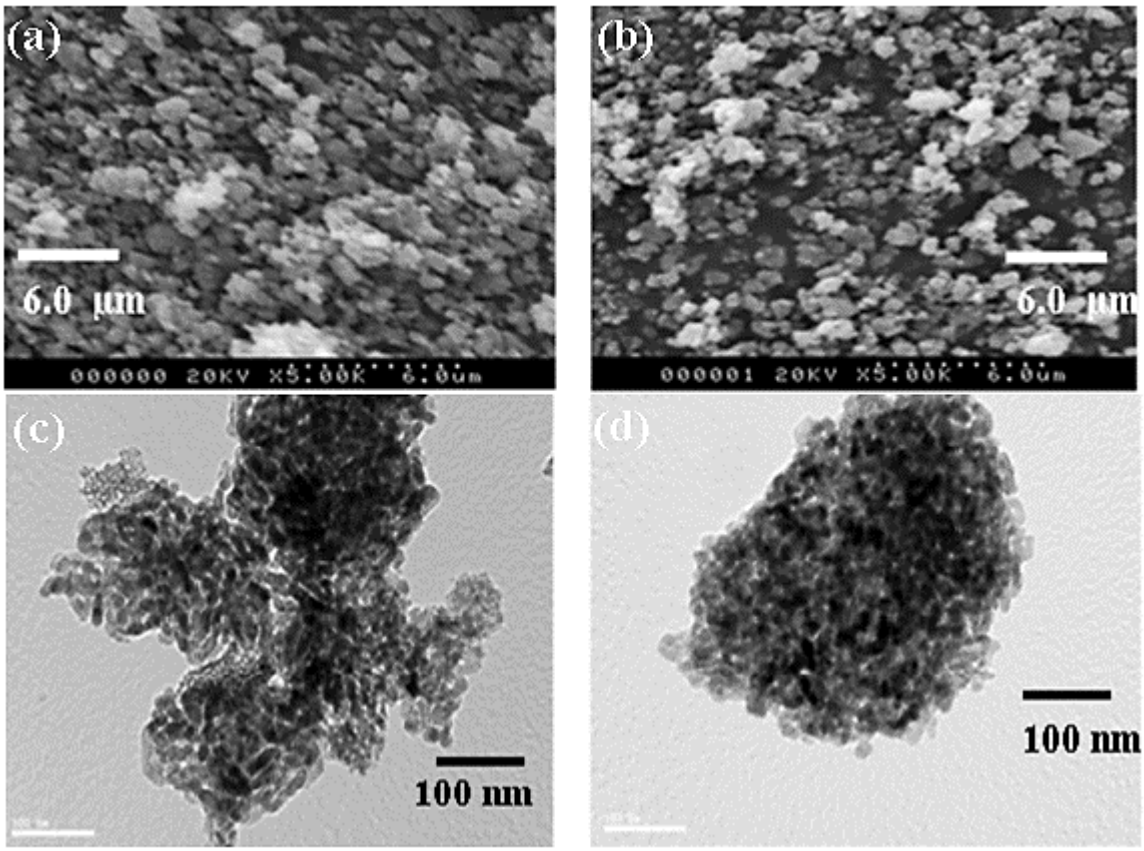

Figure 5 – SEM (a and b) and TEM (c and d) images of (a) Cu/TiO_2, (b) $Cu/600TiO_2$, (c) Cu/TiO_2 and (d) $Cu/600TiO_2$.

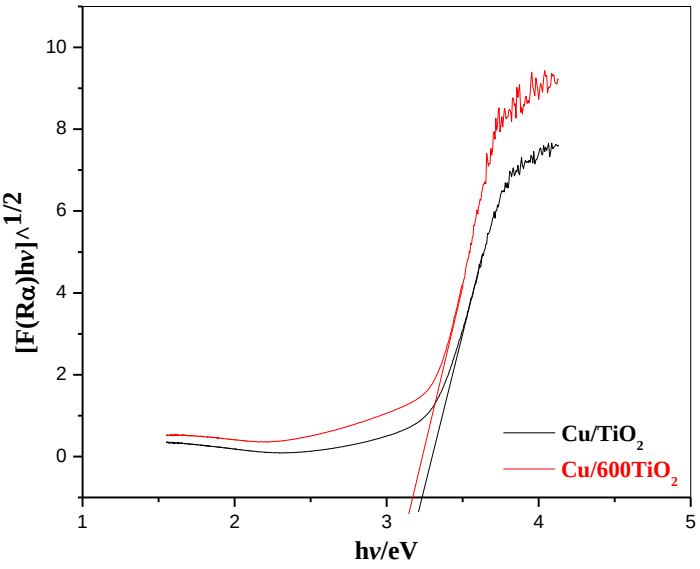

Figure 6 - UV-vis absorbance measurement of Cu/TiO_2 and $Cu/600\text{-}TiO_2$.

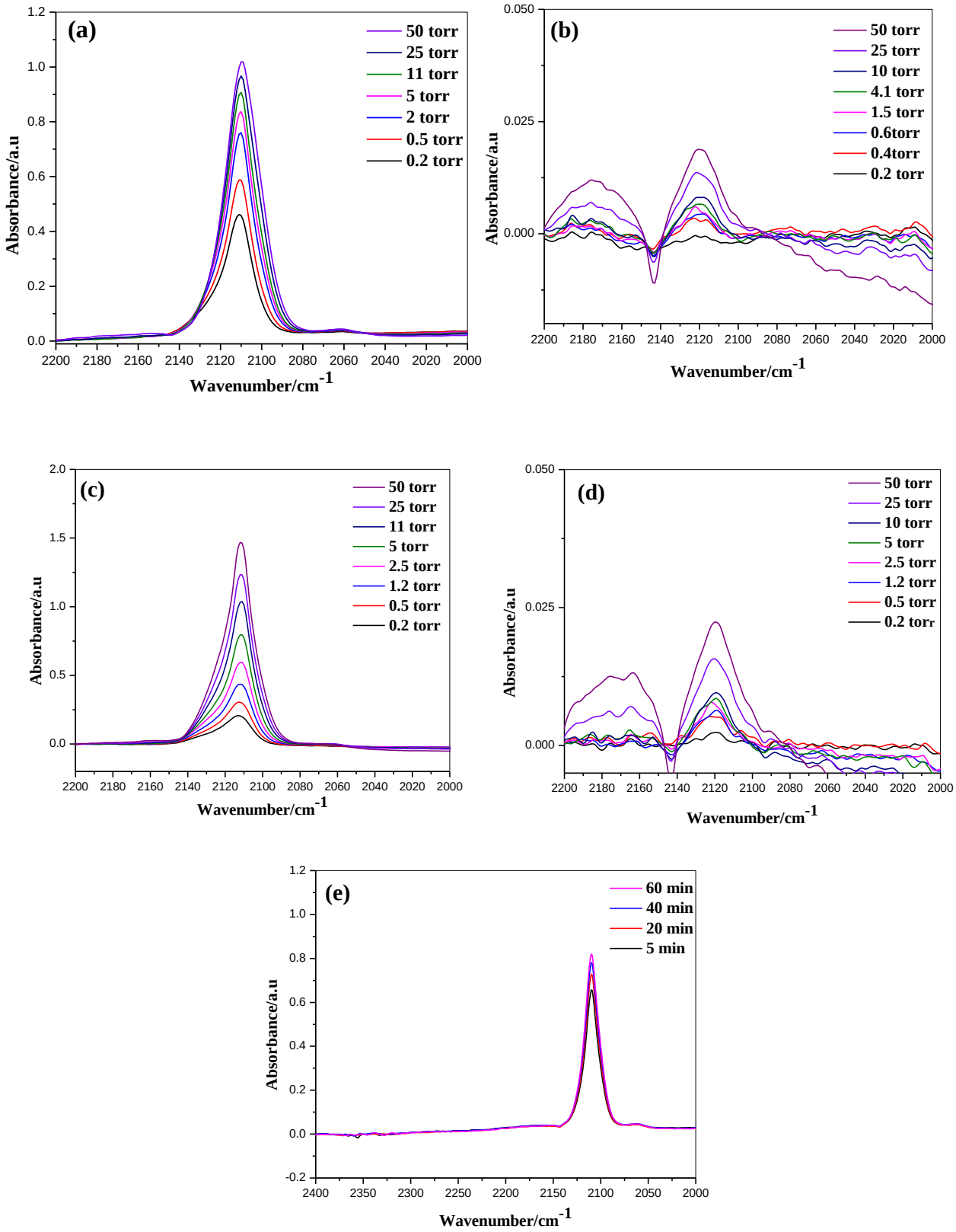

Figure 7 - FTIR spectra of CO adsorbed on (a) $Cu/600TiO_2$, (b) Cu/TiO_2, (c) $Cu_2O/600TiO_2$, (d) Cu_2O/TiO_2 and (e) $Cu/600TiO_2$ exposed to CO at beam temperature as a function of time.

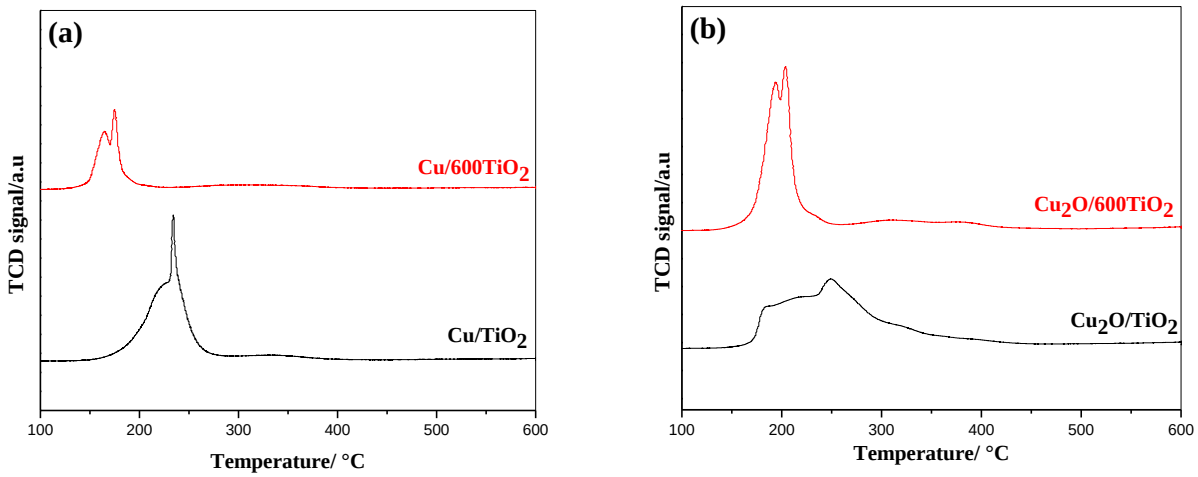

Figure 8- TPR profiles of (a) Cu/TiO_2 and $Cu/600TiO_2$ and (b) Cu_2O/TiO_2 and $Cu_2O/600TiO_2$.

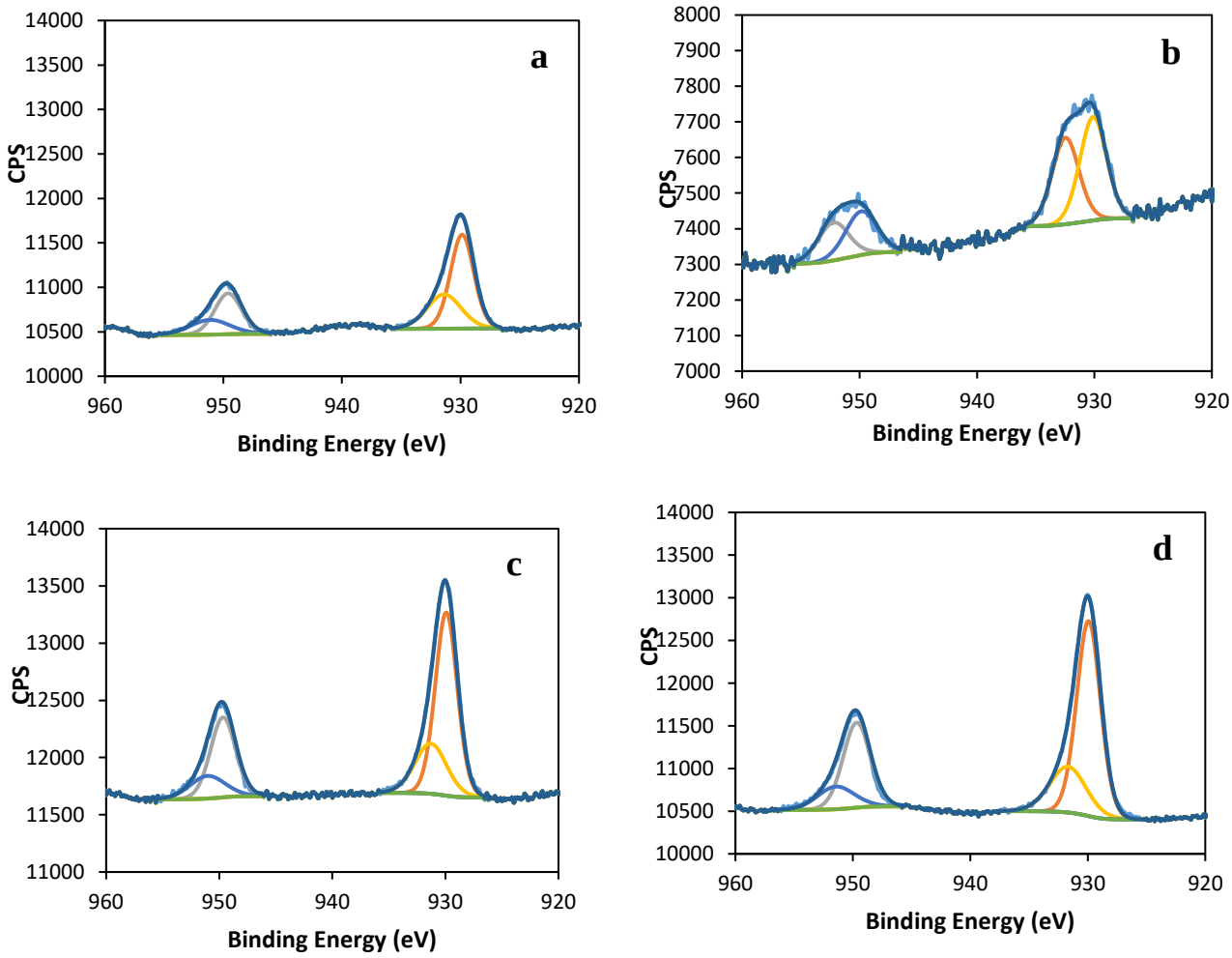

Figure 9 – XP Spectra of (a) Cu/TiO_2, (b) $Cu/600TiO_2$, (c) Cu_2O/TiO_2, and (d) $Cu_2O/600TiO_2$.

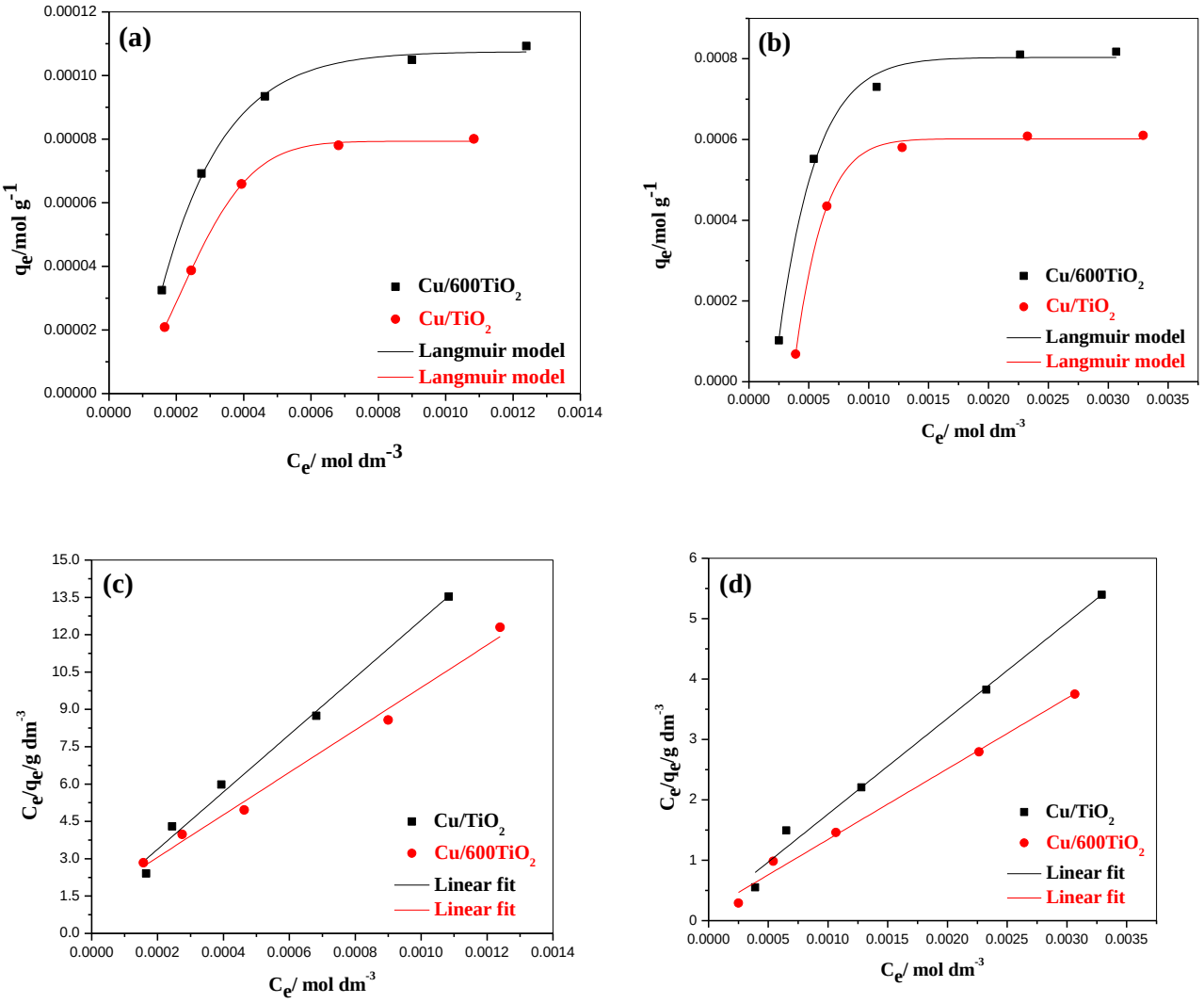

Figure 10 - Adsorption isotherms of (a) nitrate and (b) oxalic acid, on Cu/TiO_2 and $Cu/600TiO_2$, and (c-d) their corresponding data fit to Langmuir expression.

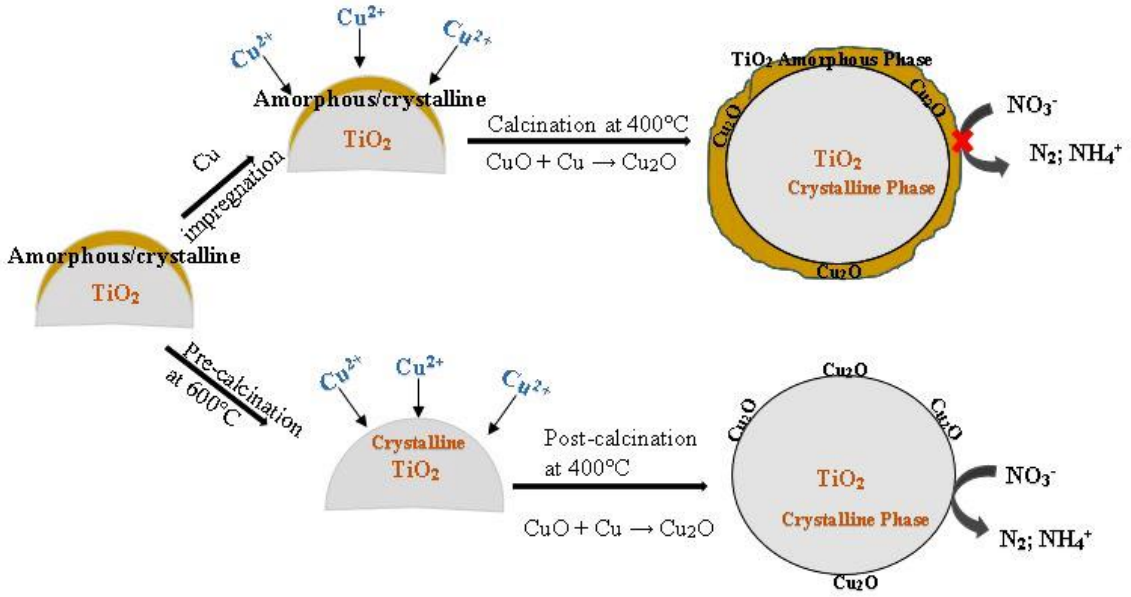

Scheme 1- Model of Cu promoted TiO_2 with mixed amorphous/crystalline and crystalline phase structures.

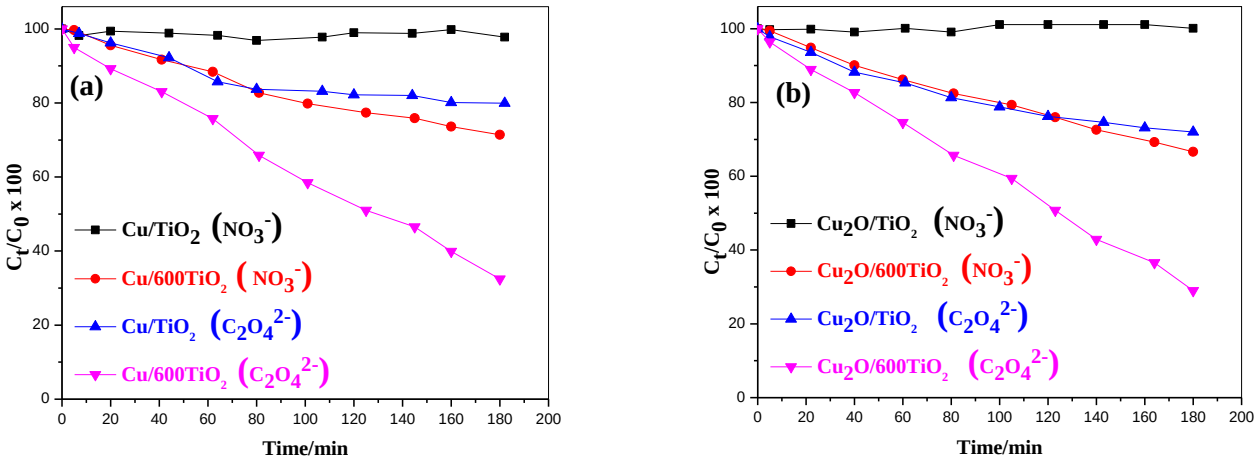

Figure 11 - Simultaneous photocatalytic remediation of nitrate and oxalic acid over (a) Cu/TiO_2 and $Cu/600TiO_2$, (b) Cu_2O/TiO_2 and $Cu_2O/600TiO_2$.

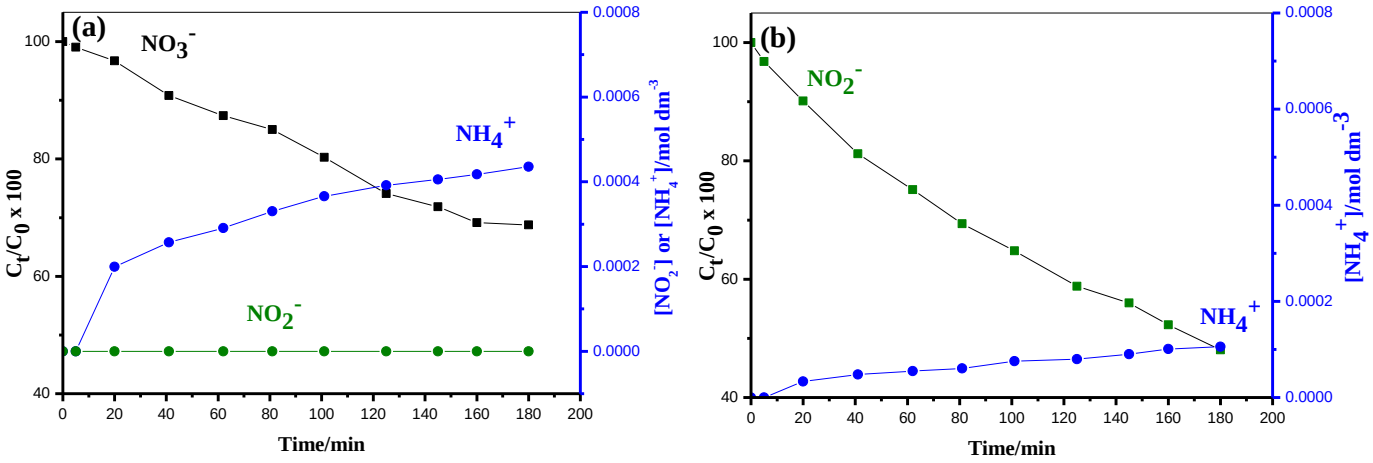

Figure 12 – Concentration profiles of photoreduction of (a) NO_3^- and (b) NO_2^- along with corresponding products profiles (NH_4^+) over Cu/600TiO_2.

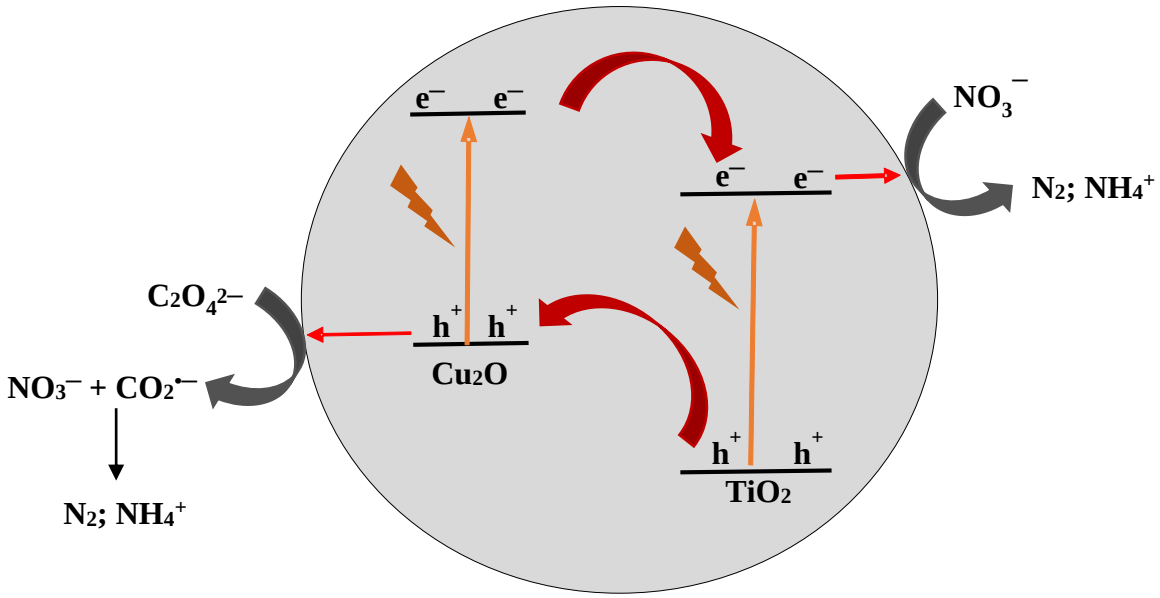

Scheme 2- Proposed simultaneous photoremediation of nitrate and oxalic acid over Cu promoted TiO_2 photocatalyst.